UNIVERSITY of CALIFORNIA
SANTA CRUZ

THERMAL EVOLUTION OF URANUS AND NEPTUNE WITH CONDENSATION-INHIBITED CONVECTION

A thesis submitted in partial satisfaction of the
requirements for the degree of

BACHELOR OF SCIENCE

in

ASTROPHYSICS

by

Robert Schroder

February 2021

Abstract

Thermal Evolution of Uranus and Neptune with Condensation-inhibited Convection

by

Robert Schroder

Voyager 2 data appears to show that Uranus has no intrinsic flux. Contemporary, dry adiabatic models predict a warmer Uranus at present time. We examine under what conditions stable water condensation zones would form in the hydrogen dominated atmospheres of our solar system ice giants. We study these stable condensation zones in the context of an interior structure model that departs from conventional dry-adiabatic models by including a moist adiabatic interior. We investigate how stable water condensation zones impact the warming of the interior, and what impact the presence of these zones have on the thermal evolution of the ice giants. We find that the existence of stable water condensation zones do not explain the problem of Uranus having no intrinsic temperature at present time. We also find that a moist adiabatic interior with the inclusion of stable water condensation zones result in a warmer Uranus and Neptune at present time than predicted by models with simple dry adiabatic or moist adiabatic interiors.

Contents

List of Figures

1

Introduction

According to core accretion theory, planets coalesce from matter contained within their parent star's protoplanetary disk. A planet will accrete matter from the disk until the supply of matter has been exhausted, at which point, the planet will begin to cool and contract over time (Lissauer & Stevenson, 2007; Armitage, 2013). It is natural to ask, what is a planet's temperature as it cools? Are we talking about the temperature at the surface? What do we mean by surface? How does energy get transported through the planet's interior? Does it conduct, convect, radiate, or all of these? If so, where, and under what conditions? Do clouds form, and do they impact a planet's cooling trajectory? These are some of the questions that physicists attempt to answer when modeling giant planet interiors and atmospheres. The sections in this first chapter will begin by reviewing some of thermodynamic concepts relevant to the physics of giant planet interiors, and will close with a brief overview of the observations and prior work on interior structure models that specifically motivated this work. In Chapter 2, we'll describe a conventional model for ice giant interior structure, and how our moist-convective model differs. We present our results in Chapter 3, describing where and when stable water condensation zones form, how they impact cooling within the interior, and their impact on thermal evolution. In Chapter 4, we discuss our conclusions and offer suggestions for future work.

1.1 Relevant Thermodynamics

1.1.1 Temperatures

There are several temperatures we are concerned with. Beginning with the effective temperature,$T_{\rm eff}$, which is defined in terms of the total flux, F_P, integrated over all frequencies, ν, of a black body of the same shape and same distance as the planet (Seager, 2010):

$$F_P = \int_0^\infty F_P(\nu)d\nu = \pi\int_0^\infty B(T,\nu)d\nu = \sigma_{\rm B}T_{\rm eff}^4, \tag{1.1}$$

where σ_B is the Stefan-Boltzmann constant. Solving for $T_{\rm eff}$ yields

$$T_{\rm eff} = \left(\frac{F_{\rm P}}{\sigma_{\rm B}}\right)^{\frac{1}{4}}. \tag{1.2}$$

The equilibrium temperature, $T_{\rm eq}$, is the temperature the planet would have if it were in thermal equilibrium with its parent star. This occurs when the planet has radiated away its latent heat of formation, and the only remaining source of energy is from its star. This temperature is estimated as

$$T_{\rm eq} = (T_{\rm eff\star})\left(\frac{R_\star}{a}\right)^{\frac{1}{2}}[f(1-A_B)]^{\frac{1}{4}}, \tag{1.3}$$

where $T_{\rm eff\star}$ is the effective temperature of the parent star, $R_\star$ is the star's radius, and a is the semi-major axis of the planet's orbit. The factor $(1 - A_{\rm B})$ is the the fraction of energy from the parent star absorbed by the planet's atmosphere, A_B, being the bond albedo, which represents the fraction of the parent star's incident energy that is reflected back into space. The factor f accounts for the planet's distribution of the radiation it receives from its parent star. We make the assumption assumption that for Neptune and Uranus that the Sun's radiation is evenly distributed throughout, and thus $f = 1$.

Finally, the intrinsic temperature, $T_{\rm int}$, is the temperature that defines the flux from the planet's interior and is defined by the relation

$$T_{\rm eff}^4 = T_{\rm eq}^4 + T_{\rm int}^4. \tag{1.4}$$

1.1.2 Energy Transport

How energy flows throughout a planet's interior impacts its actual vertical temperature structure, known as the temperature gradient, defined as

$$\nabla_T = \frac{d\ln T}{d\ln P}, \tag{1.5}$$

where T is temperature and P is pressure. In this section, we'll review the relevant modes of energy transport within a giant planet's interior and discuss the criteria for convection and condensation to occur.

Convection is a common form of energy transport within the interior of giant planets. In convecting regions, the interior is treated as parcels of compressible gases or fluids. A parcel will compress or expand without exchanging heat with its surroundings. When there is no heat exchange, the process is said to be 'adiabatic'. As a parcel of gas rises, its temperature decreases while its volume increases. This process is known as adiabatic expansion. Conversely, if the parcel sinks, it gets warmer as its volume decreases. This process is known as adiabatic compression. These processes assume constant entropy. It is said that the temperature-pressure profile follows a dry adiabatic gradient, or dry lapse rate (R. Kippenhahn, 2012), given by

$$\nabla_{\rm ad} = \left(\frac{\partial \ln T}{\partial \ln P} \right)_{\rm s}, \tag{1.6}$$

where s is entropy. The vertical temperature structure can also be expressed in terms of temperature and altitude (Sanchez-Lavega, 2010) as

$$\frac{dT}{dz} = \frac{-g}{C_P} = \Gamma_{\rm dry}, \tag{1.7}$$

where z is the altitude, and C_P is specific heat. To determine whether a layer is dynamically unstable in a region of homogeneous chemical composition, we use the Schwarzschild & Harm criterion (R. Kippenhahn, 2012) as the criterion for convection, defined as

$$\nabla_T > \nabla_{\rm ad}. \tag{1.8}$$

In a region that does not have a homogeneous chemical composition, but rather has a gradient in mean molecular weight, defined as

$$\nabla_\mu = \frac{d \ln \mu}{d \ln P}, \tag{1.9}$$

we use the Ledoux criterion(R. Kippenhahn, 2012)

$$\nabla_T > \nabla_{\rm ad} + \frac{\rho}{\delta} \nabla_\mu, \tag{1.10}$$

where

$$\rho = \left(\frac{\partial \ln \rho}{\partial \ln \mu} \right)_{\rm P,T} \tag{1.11}$$

and

$$\delta = - \left(\frac{\partial \ln \rho}{\partial \ln T} \right)_{\rm P,\mu}. \tag{1.12}$$

Condensation can also have a large impact on a planet's energy balance. For example, the presence of clouds can change a planets albedo. The condensation of vapor results in the release of energy. So, it is important consider the presence of condensible species when modeling the interior of giant planets. Gases condense at at sufficiently low temperatures or high pressures. Condensation of a gas is characterized by its saturation vapor pressure, which derives from the Clausius-Clapeyron equation (Lavega, 2011). The saturation vapor pressure, $P_{\rm sat}$, is given by

$$P_{\rm sat}(T) = P_{\rm sat}(T_0)e^{-\frac{L+C_{\rm p}T_0}{R_{\rm vap}}(\frac{1}{T}-\frac{1}{T_0})-\frac{C_{\rm p}}{R_{\rm vap}}\ln\frac{T}{T_0}} \tag{1.13}$$

where $T_0 = 273.16K$, and $R_{\rm vap}$ is the gas constant for the condensible species, and L is the latent heat of vaporization for the condensate. When the partial pressure of a gas, $P_{\rm gas}$, is less than $P_{\rm sat}$, the parcel of gas is 'subsaturated'. When $P_{\rm gas} = P_{\rm sat}$, the gas is 'saturated'. And, when $P_{\rm gas} > P_{\rm sat}$, the parcel is 'supersaturated'. Every condensible species has its own saturation vapor pressure. We define the moist adiabat as (Lavega, 2011)

$$\nabla_{\rm moist} = (1 + \frac{\frac{x_{\rm vap}L}{R_{\rm vap}T}}{\nabla_{ad} + \frac{L^2}{R_{\rm vap}^2T^2}}) \tag{1.14}$$

where $x_{\rm vap}$ is the vapor mole fraction defined as

$$x_{\rm vap} = \frac{P_{\rm sat}}{P}. \tag{1.15}$$

Within the condensation zone, the vapor mole fraction, $x_{\rm vap}$, is equal to the saturated vapor mole fraction:

$$x_{\rm vap} = x_{\rm vap}^{\rm sat} = \frac{P_{\rm sat}}{P}, \qquad P_{\rm top} < P < P_{\rm base}. \tag{1.16}$$

Condensation on Earth is notably different from condensation that occurs in hydrogen dominated atmospheres. On Earth, as a parcel of air is lifted, it cools until it gets cold enough that water vapor condenses out, releasing latent heat of condensation which further boosts convection. This release of energy alters the temperature-pressure profile of the atmosphere, which now follows a moist adiabat. In addition to altering the temperature gradient, condensation may also create a gradient in mean molecular weight. For example, on Earth, moist air is lighter than dry air. H_2O vapor (molecular mass = 18 g/mol), the primary condensate in Earth's atmosphere, is lighter (not by much) than the background air which is composed primarily of N_2 (molecular mass = 28 g/mol). When H_2O vapor abundance exceeds the saturation vapor pressure, the vapor condenses out of the atmosphere, resulting in a small vertical gradient in mean molecular weight. In Earth's atmosphere, this small gradient does not impose a significant barrier to convection. By contrast, in hydrogen dominated atmospheres such as Neptune and Uranus, the background gas is much lighter than the condensates. In this hydrogen-rich environment, when H_2O condenses out of the atmosphere, a strong vertical gradient in mean molecular weight can be established, resulting in a negative buoyancy for the convecting parcel of gas. This can create a situation where the zone in which water condenses is stable against convection (Guillot, 1995), (Friedson & Gonzales, 2017), (Leconte et al., 2017).

Thus far, we have been discussing H_2O as the only condensate. However, other condensates such as NH_3 and CH_4 may impact convection as well. In this study, we only consider H_2O as the primary condensate as it likely has the largest impact. The reason for this is that if its abundance is supercritical, then it results in a larger superadiabicity (larger temperature gradient) than would be provided by either NH_3 r CH_4 (Guillot, 1995). Consideration of other condensates is planned for future work.

1.2 Prior Work

In 1965, Frank Low measured Jupiter's intrinsic temperature (Low, 1966). To explain this observation, theorists set out to expand on the seminal work by (Demarcus, 1958) on the theory of interior structure of solar system giant planets (Hubbard, 1968; Smoluchowski, 1967; Hubbard, 1977, 1978; M. Podolak, 1991). In 1968, it was Hubbard who showed that a convective interior would allow Jupiter's observed flux to be transported to the surface adiabatically. This analysis motivated the inclusion of dry adiabatic interiors in contemporary interior structure models for gas and ice giants.

At the present time, most of the giant planets in our solar system: Saturn, Jupiter, and Neptune, all have an observed intrinsic flux. Uranus is the exception (Pearl & Conrath, 1991). Measurements of Uranus's effective temperature are consistent with a planet that has no intrinsic flux, a planet in thermal equilibrium with the Sun, cooler than its more distant neighbor, Neptune, a planet of similar mass and composition. The observed effective temperatures and estimated equilibrium temperatures for the giant planets are listed in Table 1.1.

While thermal evolution models do currently reproduce T_{eff} for Jupiter and Neptune at 4.6 Gyr (Graboske et al., 1975; Fortney et al., 2011), they do not reproduce T_{eff} for Saturn and Uranus. Models for Saturn predict a cooler planet; however, plausible explanations have been offered to explain its current, warmer T_{eff}. Among them, the rain-out of helium (Fortney & Hubbard, 2003; Mankovich & Fortney, 2019), or double-diffusive convection (Leconte & Chabrier, 2013).

Meanwhile, for Uranus, the models have predicted a warmer effective temperature at present time (Fortney et al., 2011; M. Podolak, 1991; W.B. Hubbard, 1995; L. Scheibe,

Planet	Effective Temperature [K]	Equilibrium Temperature [K]
Jupiter	124.4 ± 0.3	109
Saturn	95.0 ± 0.4	80
Uranus	59.1 ± 0.3	58
Neptune	59.3 ± 0.8	49

Table 1.1: Temperatures of Giant Planets [Adapted from (Seager, 2010)]

2019). There have been various attempts to explain Uranus's luminosity anomaly. Early investigations posited that a stratified interior, stable against convection, would allow heat to be trapped deep within the the interior (M. Podolak, 1991). Later work investigated some of the other possible explanations for Uranus's cool temperature. (Guillot, 1995) posited that condensates such as NH_3, CH_4, or H_2O when at critical abundance could interfere with convection, producing temperature profiles that would be superadiabatic. (Nettelmann et al., 2016) looked at the inclusion of ad-hoc thermal boundary layers within a planet's interior and found that they could possibly explain Uranus's current T_{eff}. Both (Friedson & Gonzales, 2017) and (Leconte et al., 2017) explored the impact of condensates forming stable radiative layers. Both carried out linear stability analyses and reached similar findings, concluding that super-critical abundances of H_2O would result in a superadiabatic temperature gradient. All of these investigations showed that the presence of thermal boundary layers could possibly provide a mechanism to trap heat deep within the interior, allowing the envelope above to cool more rapidly.

The work done by (Guillot, 1995), (Friedson & Gonzales, 2017), and (Leconte et al., 2017) examined under what conditions stable condensation zones would form in hydrogen dominated atmospheres. In this paper, we apply the same physical mechanisms for the formation of stable water condensation zones. However, we expand on this by placing these stable, radiative layers in the context of a more complete model of interior structure for solar system ice giants. Finally, we investigate how these stable layers impact the cooling of the planets over time.

2

Model

2.1 Differential Equations for Structure and Evolution

We begin our description of the physics of our interior structure model by assuming that we are dealing with a spherically symmetric object with no electromagnetic field. With these assumption in place, we employ the following equations to describe the interior and evolution of ice giants.

Conservation of Mass

$$\frac{dm}{dr} = 4\pi r^2 \rho, \tag{2.1}$$

where dm is the mass contained within a sphere of radius $r + dr$, and ρ is the density.

Hydrostatic Equilibrium

$$\frac{dP}{dr} = -\frac{Gm\rho}{r^2}, \tag{2.2}$$

where P is the pressure and G is the gravitational constant.

Conservation of Energy

Conservation of energy implies that the planet's luminosity, $L = 4\pi R^2 \sigma_B T_{\text{int}}^4$, must be balanced by the rate of change of its total internal energy. When we have a sequence of progressively cooler models, we calculate the time-step between any two models using the energy conservation equation as in (Fortney et al., 2011)

$$\frac{dL}{dm} = -T\frac{\partial S}{\partial t}, \tag{2.3}$$

where dm is the mass of the shell, ∂S is the entropy of the shell, and T is the temperature of the shell. Solving for ∂t, we get the time-step

$$\partial t = -\frac{1}{L}\int_0^M \partial S\, dm. \tag{2.4}$$

2.2 Standard Interior Structure Model

Inputs

We employ a three-layer interior structure, seen schematically in Figure 2.1. Broadly speaking, we assume a water 'ice' core. There is an inner envelope that is composed mostly of H_2O, with trace amounts of H and He. We have left out other ices such as NH_3 and CH_4. The outer envelope is dominated by hydrogen and helium, with trace amounts of water,

Planet	m_{core} ($m_\oplus$)	m_{12} ($m_\oplus$)	X_2 (mass fraction)	Y_2 (mass fraction)	Z_2 (mass fraction)
Uranus	1.51	12.5	99.08906	0.03294	0.87800
Neptune	2.85	15.0	99.10804	0.03996	0.85200

Table 2.1: Model Input Parameters:

Planet	X_1 ($q_{deep=0.05}$)	Y_1 ($q_{deep=0.05}$)	X_1 ($q_{deep=0.15}$)	Y_1 ($q_{deep=0.15}$)	X_1 ($q_{deep=0.25}$)	Y_1 ($q_{deep=0.25}$)
Uranus	99.6935	0.2565	99.6205	0.2295	99.5475	0.2025
Neptune	99.6935	0.2565	99.6205	0.2295	99.5475	0.2025

Table 2.2: Model Input Parameters:

excluding methane and ammonia. It should be noted, that the concentration of ices in the interior of Neptune and Uranus is poorly constrained. These planets have not received the same amount of detailed observation from probes that Jupiter and Saturn have enjoyed. As such, our model inputs assume a range of deep water concentrations, from here on referred to as q_{deep}. Furthermore, the mass fraction of H_2O in the inner envelope, Z_2, is also poorly constrained.

Equations of State

Near the surface, the ideal gas law provides a good approximation for relating pressure, temperature, density, and composition. However, at depth where pressure can be on the order of 10^{11} to 10^{12} bars, this approximation is no longer valid. We use (Chabrier et al., 2019) as our H-He equation of state. For water, we use (S. Mazevet & Potekhin, 2019) EOS.

Relative Mass Abundances Within Each Layer

X, Y, and Z represent mass fractions for hydrogen, helium, and water, respectively. In general

$$X + Y + Z = 1. \tag{2.5}$$

Y' is the He mass fraction relative to He + H, such that

$$Y' = \frac{Y}{X + Y}, \tag{2.6}$$

Referring to Figure 2.1, the center of the planet has a core of mass, m_{core}. The core is made of pure water ice, indicated by $Z = 1$, the H_2O mass fraction. Moving outward, the inner envelope is H_2O dominated, where Z_2 is the H_2O mass fraction, X_2, and Y_2 are the hydrogen and helium mass fractions, respectively. The outer envelope, below 1 bar, contains trace amounts of H_2O, but is mostly comprised of hydrogen and helium, with mass fractions equal to X_1 and Y_1, respectively. m_{12} is the mass coordinate that indicates the transition between the inner and outer envelope. T_1 is the temperature at $P = 1$ bar.

We use the additive-volume approximation to determine total density, given by the relation

$$\frac{1}{\rho} = \frac{1 - Z}{\rho_{\mathrm{HHe}}} + \frac{Z}{\rho_{\mathrm{Z}}}. \tag{2.7}$$

Internal energy, u, is given by

$$u = (1 - Z)(u_{\mathrm{HHe}}) + (Z)(u_{\mathrm{Z}}), \tag{2.8}$$

where

$$u_{\mathrm{HHe}} = (1 - Y')(u_{\mathrm{H}}) + (Y')(u_{\mathrm{He}}). \tag{2.9}$$

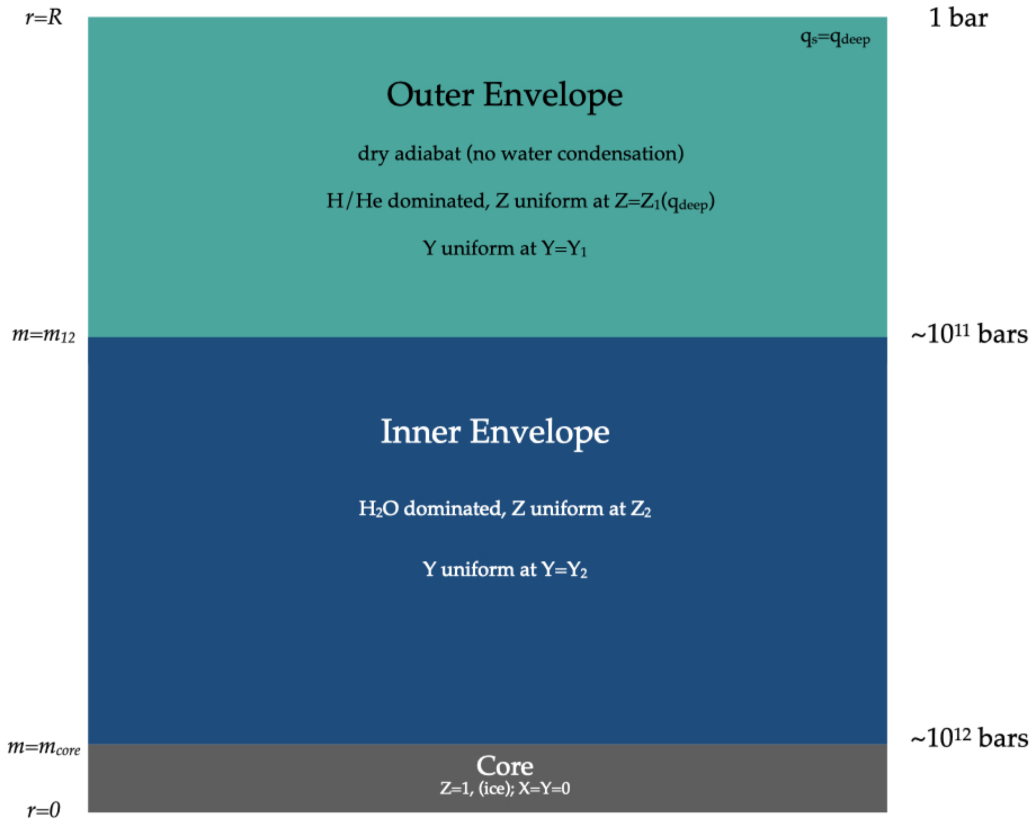

Figure 2.1: A conventional interior structure: In this model, the inner and outer envelopes are assumed to be well mixed, fully convective, and following a dry adiabat. The core is composed of water ice. The inner envelope is water dominated, with uniform concentrations of hydrogen, helium, and water; whereas, the outer envelope is hydrogen and helium dominated with trace amounts of water. The atmosphere extends beyond 1 bar, but pressures beyond 1 bar are sufficient to capture the formation and impact of the water condensation zones investigated here.

Model Atmosphere

Finally, beyond the outer envelope is the atmosphere. Atmospheres regulate how quickly the energy within a planet's interior can radiate into space. When modeling the thermal evolution of gas and ice giants, it has long been recognized that model atmospheres constitute an outer boundary condition for interior structure models, providing key inputs that impact cooling times for interior structure models (Graboske et al., 1975; Fortney et al., 2011). Specifically, model atmospheres allow us to link the planet's $T_{\rm int}$ and $T_{\rm eff}$ to the model's surface gravity, g, and its T_1 or T_{10}. Our work utilizes the (Fortney et al., 2011) model atmosphere.

2.3 Inclusion of Moist Adiabat Within Outer Envelope of Standard Model

Our interior structure model modifies the conventional structure described in Section 2.1 by adding a moist adiabatic layer to the outer envelope, as seen schematically in Figure 2.2, which under favorable conditions, allows for the condensation of H_2O.

In Figure 2.3, we compare pressure-temperature and pressure-xvap profiles that follow a dry adiabatic lapse rate, a moist adiabatic lapse rate, and a moist adiabatic lapse rate containing a radiative layer at some depth. The profile of the moist adiabatic lapse rate is cooler at depth than either of the other two profiles. However, the presence of a stable radiative layer results in a warmer interior. These profiles assume $q_{\rm deep} = 0.25$ and $T_1 = 150K$, which is approximately when the onset of condensation-inhibited convection occurs, as will be shown in Chapter 3. When the pressure-temperature profile follows a dry adiabat, the vapor mole fraction, $x_{\rm vap}$, is constant.

If condensation occurs, our model assumes that it may be stable against convection if a fast rain-out occurs such that the vertical gradient in mean molecular weight is large enough to counteract the positive buoyancy of the parcel of gas (Leconte et al., 2017)

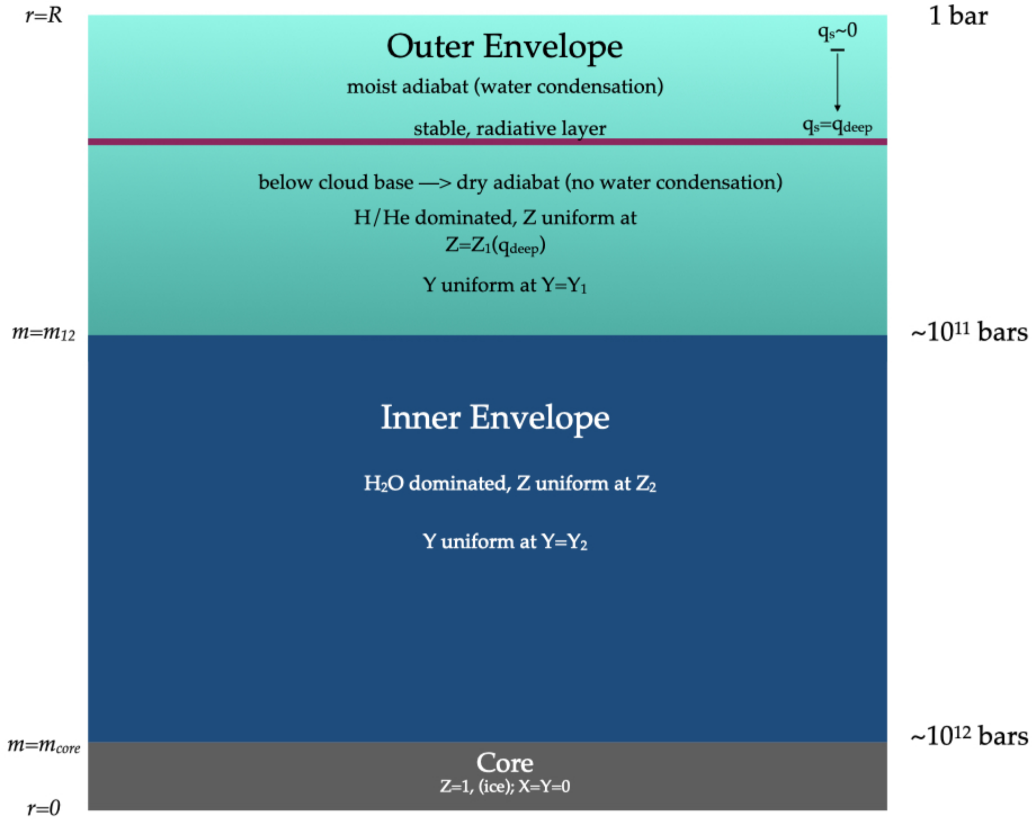

Figure 2.2: The structure for moist adiabatic interior, allowing for condensation-inhibited convection. In this model, a stable water condensation zone may form. The red horizontal line indicates the radiative zone (water condensation zone). The pressure and temperature at the base of the condensation zone is set by the condition that x_{vap} has reached the deep value $x_{\text{vap}}^{\text{deep}}$. Below the condensation zone, the temperature and pressure follow a dry adiabat.

(Friedson & Gonzales, 2017). In this scenario, convection is interrupted when α, which is derived from Equation 1.10, is negative. α (Friedson & Gonzales, 2017) is given by

$$\alpha = 1 + \xi(q_s L/R_{\text{vap}} T_0), \tag{2.10}$$

where R_{vap} is the gas constant for the vapor (water), T_0 is the local temperature, L is the

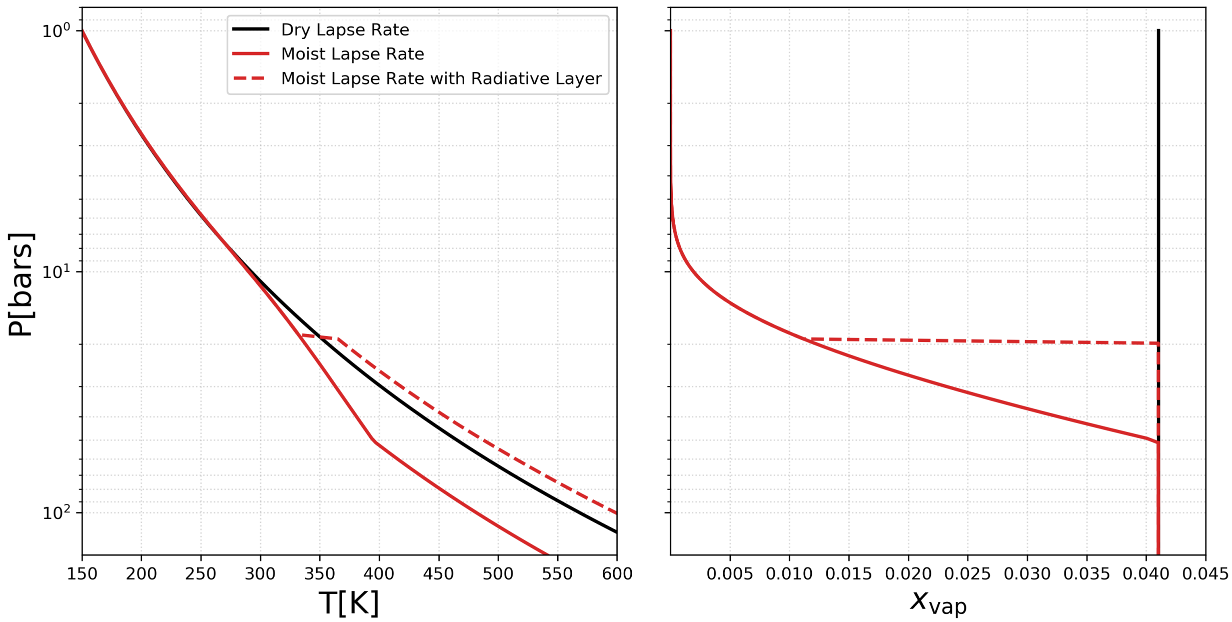

Figure 2.3: The solid red line is the profile following moist adiabatic lapse rate. The solid black line is following the the dry adiabatic lapse rate. The dashed red line is following a moist adiabatic lapse rate with the addition of a stable radiative layer (water condensation zone).

latent heat of vaporization for water, q_s is the saturation specific humidity, and ξ is given by $\xi = \frac{1}{\epsilon} - 1$, where ϵ is the ratio of the molecular weight of vapor to the mean molecular weight of dry atmosphere. In our case, $\xi \approx -0.872$. When α is negative, the vertical gradient in molecular weight results in a stabilizing effect, overwhelming the effects due to latent heat release.

Temperature Jump Across the Water Condensation Zone

In a layer in which alpha, Eqn. 2.10, becomes negative, convection is interrupted. In the limit that H_2O rains out quickly, (Friedson & Gonzales, 2017; Leconte et al., 2017) it has been shown that radiative diffusion is responsible for heat transport within the zone, with the temperature gradient across the zone following a radiative temperature gradient

(R. Kippenhahn, 2012)

$$\nabla_{\mathrm{rad}} = \frac{3}{16}\frac{\kappa_{\mathrm{R}} P}{g}\frac{T_{\mathrm{int}}^4}{T^4}. \tag{2.11}$$

Due to the large opacities, κ_{R}, that are typical of giant planet interiors, the radiative gradient is significantly larger than the either the dry adiabatic gradient or moist adiabatic gradient. Since our model has a finite radial resolution, it is unable to spatially resolve the temperature change. Instead, the model treats the water condensation zone (a thin, stable, radiative layer) as a discontinuous increase in temperature. Nevertheless, this radiative zone corresponds to a continuum of temperatures that is governed by

$$T(P) = T_{\mathrm{top}} + \int_{P_{\mathrm{top}}}^{P_{\mathrm{base}}} \left(\frac{dT}{dP}\right)_{\mathrm{rad}} dP, \tag{2.12}$$

with P_{top} and T_{top} denote the pressure and temperature at the top of the stable water condensation zone, and P_{base} represents the bottom of the zone. The radiative temperature gradient across the water condensation zone is nearly constant, so that Eqn. 2.12 simplifies to

$$T_{\mathrm{base}} \equiv T(P + \Delta P) = T_{\mathrm{top}} + \left(\frac{dT}{dP}\right)_{\mathrm{rad}} \Delta P, \tag{2.13}$$

where ΔP is the extent of the pressure-space of the water condensation zone (radiative layer), given by

$$\Delta P \equiv P_{\mathrm{base}} - P_{\mathrm{top}} = \frac{P_{\mathrm{sat}}(T_{\mathrm{base}})}{x_{\mathrm{vap}}^{\mathrm{deep}}} - P_{\mathrm{top}}. \tag{2.14}$$

Within the condensation zone, the vapor mole fraction, x_{vap} is equal to the saturated vapor mole fraction:

$$x_{\mathrm{vap}}(P,T) = x_{\mathrm{vap}}^{\mathrm{sat}}(P,T) = \frac{P_{\mathrm{sat}}(T)}{P}, \qquad P < P_{\mathrm{base}}. \tag{2.15}$$

The base of the condensation zone is set by the condition that x_{vap} has reached the deep value $x_{\mathrm{vap}}^{\mathrm{deep}}$:

$$x_{\mathrm{vap}}^{\mathrm{sat}}(P_{\mathrm{base}}, T_{\mathrm{base}}) = \frac{P_{\mathrm{sat}}(T_{\mathrm{base}})}{P_{\mathrm{base}}} = x_{\mathrm{vap}}^{\mathrm{deep}}. \tag{2.16}$$

Below the water condensation zone, the region is subsaturated and hence no condensation occurs. Temperatures below the water condensation zone are obtained by integrating the dry adiabat ∇_{ad}

$$T(P) = T_{\mathrm{base}} + \int_{P_{\mathrm{base}}}^{P} \left(\frac{dT}{dP}\right)_{\mathrm{ad}} dP, \qquad P > P_{\mathrm{base}}. \tag{2.17}$$

3

Results

3.1 Condensation-inhibited Convection

In Figure 3.1, we show the results of our initial, exploratory models. We show α with respect to pressure, vapor mole fraction, and temperature. These static models are run for a variety of T_{10}'s, the planet's temperature at $P = 10$ bars. As the bulk water abundance for Uranus and Neptune is unconstrained (Guillot, 1995), these model runs use three different values of q_{deep}, for the purpose of searching for deep water abundances and evolutionary phases for which convection is inhibited by water condensation. In these exploratory models, we only consider the model Uranus. We find that for $q_{\mathrm{deep}} = 0.05$, no condensation-inhibited convection occurs. In other words, α (Eqn. 2.10) never takes on negative values with this concentration of water vapor, hence the condition for stability is never met. However, for larger values of q_{deep}, we find that α does take on negative values (see rows 2 and 3 in Figure 3.1). These finding are in agreement with (Friedson & Gonzales, 2017; Leconte et al., 2017). The shaded regions of the plots indicate the pressure-space over which α is negative. It is important to note that with these exploratory models, we neglect the stable water condensation zone's impact on the interior's thermal structure. More specifically, these profiles describe a scenario in which moist convection occurs throughout. As such, the shaded regions appear extended, when in reality the top of the shaded region indicates where the top of where the stable water condensation zone would form. As we will see in Section 2.3, self-consistent models that account for the formation of a stable zone, with a critical $q_{\rm deep}$, will show pressure-temperature profiles with an abrupt temperature increase at the location of the radiative layer. Looking at the plots for $q_{\rm deep} = 0.15$ and $q_{\rm deep} = 0.25$, we can see that condensation-inhibited convection sets in at approximately $T_{10} = 335$K. With regard to the vapor mole fraction panels on the right of Figure 3.1, we can see that for a hot model Uranus, $x_{\rm vap}$ profiles are vertical, taking on a constant value as expected. For cooler Uranus models, we see that as water condenses out, $x_{\rm vap}$ decreases. In the temperature-pressure profiles, we can see a kink in the graphs, corresponding to $x_{\rm vap}$ taking on a constant value. In other words, the region has become sub-saturated and from that point, the profile follows a dry adiabat. Finally, we can see that as the planet cools, the condensation zones descend deeper into the interior.

3.2 Formation of Radiative Zone

Now we turn our focus to static models that explicitly allow for the formation of stable water condensation zones when conditions are suitable, as determined by the stability criterion, described by Eqn. 2.10. The plots in Figure 3.3 show the temperature profile and vapor mole fraction for H_2O for three different values of $q_{\rm deep}$: 0.05, 0.15, and 0.25. In the first row, we can see that for early T_{10}'s, there is no onset of condensation, and

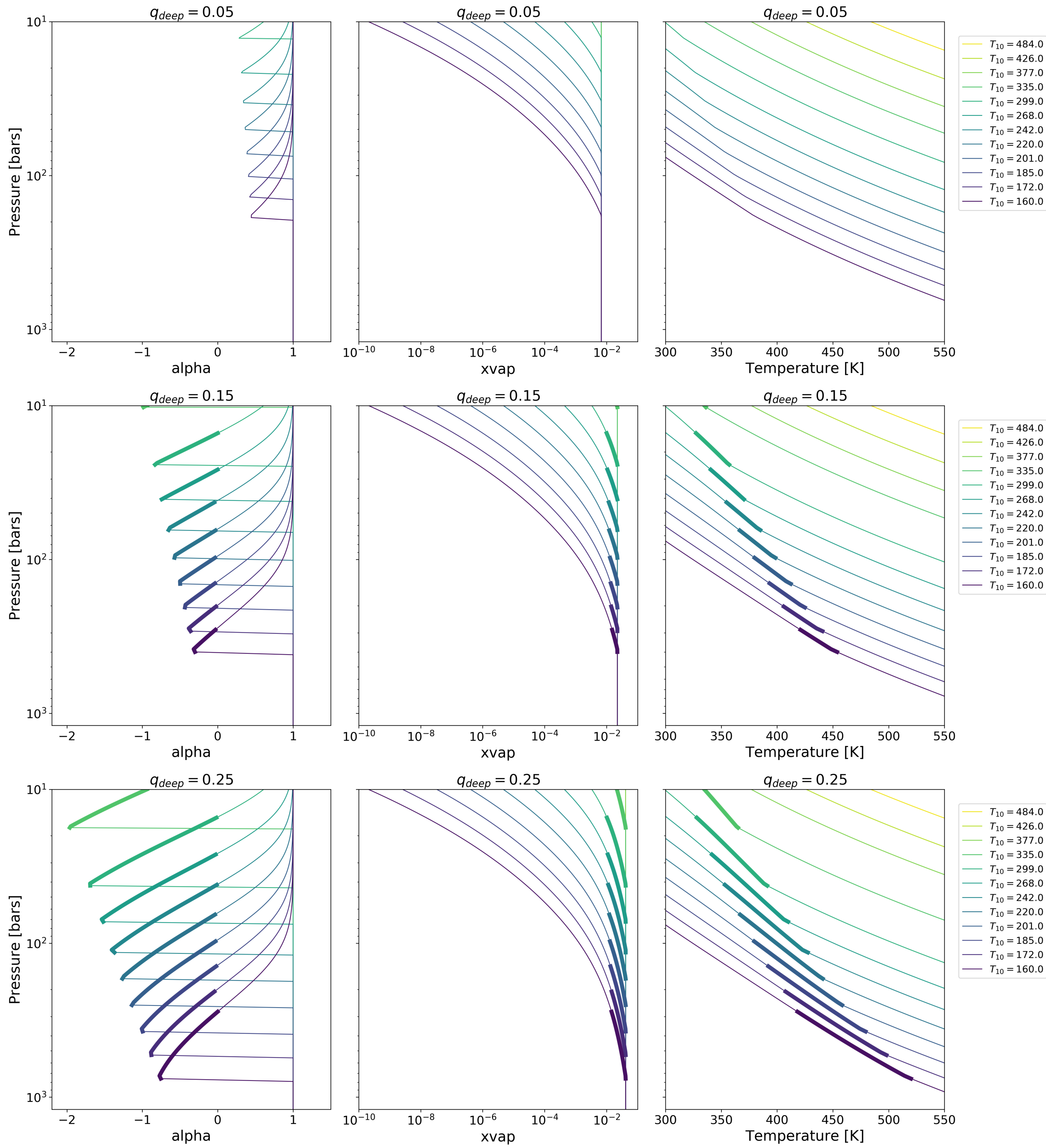

Figure 3.1: Each row represents a different value for q_{deep}. For $q_{\text{deep}} = 0.05$, no stable condensation zone forms. For $q_{\text{deep}} = 0.15$ and $q_{\text{deep}} = 0.25$, convection is inhibited by condensation. The shaded regions show the extent of when α is negative.

the profile follows a dry adiabat. For later T_{10}'s, there is a visible kink in the lapse rate which indicates the onset of condensation, at which point the lapse rate has a shallower slope. For the larger values of q_{deep}, where α takes on negative values, we see the onset of condensation-inhibited convection and the establishment of a radiative zone. In the plots, the water condensation zones are represented by the horizontal discontinuities moving from left to right. As the planet cools, these radiative zones descend deeper into the planet's interior. When the radiative zones are established, the interior below the zone becomes much warmer. In Figure 3.2, we highlight the effect of a warming interior. In this figure, we have overlaid the profiles for $q_{\text{deep}} = 0.25$ (exhibiting stable water condensation zones) over the profile for $q_{\text{deep}} = 0.05$ (no stable zones). From this plot, one can see that the presence of a radiative zone creates a temperature jump such that a given T_{10} appears to look like an earlier T_{10}. In other words, we find that the steep temperature increase caused by the presence of a radiative zone causes the interior to be much hotter than one would find using a simple moist adiabatic model with no stable layers. So, for a fixed T_{10}, while sub-critical($q_{\text{deep}} = 0.05$) and super-critical ($q_{\text{deep}} = 0.25$) models may appear identical near the surface, the super-critical model has a much warmer interior, one that resembles an earlier evolutionary track at a higher T_{10}.

Looking at the adjacent x_{vap} plots, we can see that x_{vap} follows its saturated value. At the bottom of the radiative zone, the vapor mole fraction equals its deep water value, which is the condition that sets the base of the condensation zone.

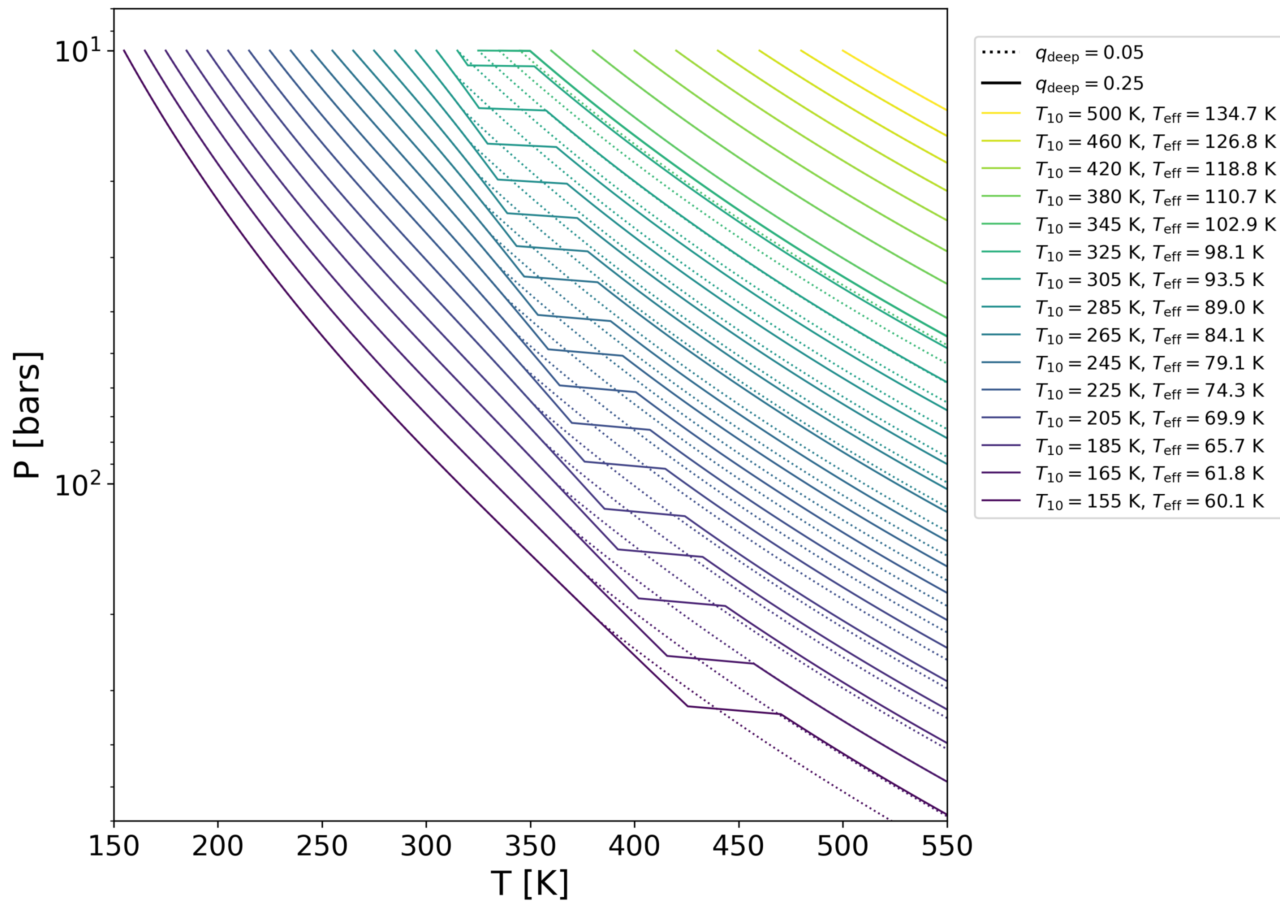

Figure 3.2: The solid lines represent the pressure-temperature profile for $q_{\mathrm{deep}} = 0.25$, and the dashed lines for $q_{\mathrm{deep}} = 0.05$. Looking at recent T_{10}'s, interior temperatures for $q_{\mathrm{deep}} = 0.25$ jump to an earlier T_{10}.

3.3 Thermal Evolution of Uranus and Neptune

In Figure 3.4, we display the results of evolutionary tracks that consider separately the evolution of a dry adiabat, a moist adiabat with condensation but no stable radiative zone, and a moist adiabat with condensation containing stable radiative zones. For all of these evolutionary tracks, we assume $q_{\mathrm{deep}} = 0.25$. The coolest scenario at present time, is a moist adiabat that is never stable against convection. The moist adiabat that allows for the formation of stable condensation zones has the warmest outcome at present time. In Figure 3.5 (Uranus) and Figure 3.6 (Neptune), we consider the impact of different concentrations of q_{deep} on the thermal evolution of Uranus and Neptune. As the planets cool, their radiative zones descend deeper into the interior, as we saw in Figure 3.3. This behavior is also noticeable in the thermal evolution plots. Looking at T_{eff} at 7×10^7 Gyr, the onset of condensation-inhibited convection occurs, resulting in a discontinuous temperature drop. The same behavior is seen in the T_{10} plots for both planets, however, by this time the radiative zone has descended deeper, later in time at around 7×10^8 Gyr. Larger deep water concentrations result in warmer Uranus and Neptune at present time. We also look at the impact of q_{deep} on the evolution of planetary radius and find that larger deep water concentrations tend to converge more closely toward the presently observed radius for both Uranus and Neptune in these simulations.

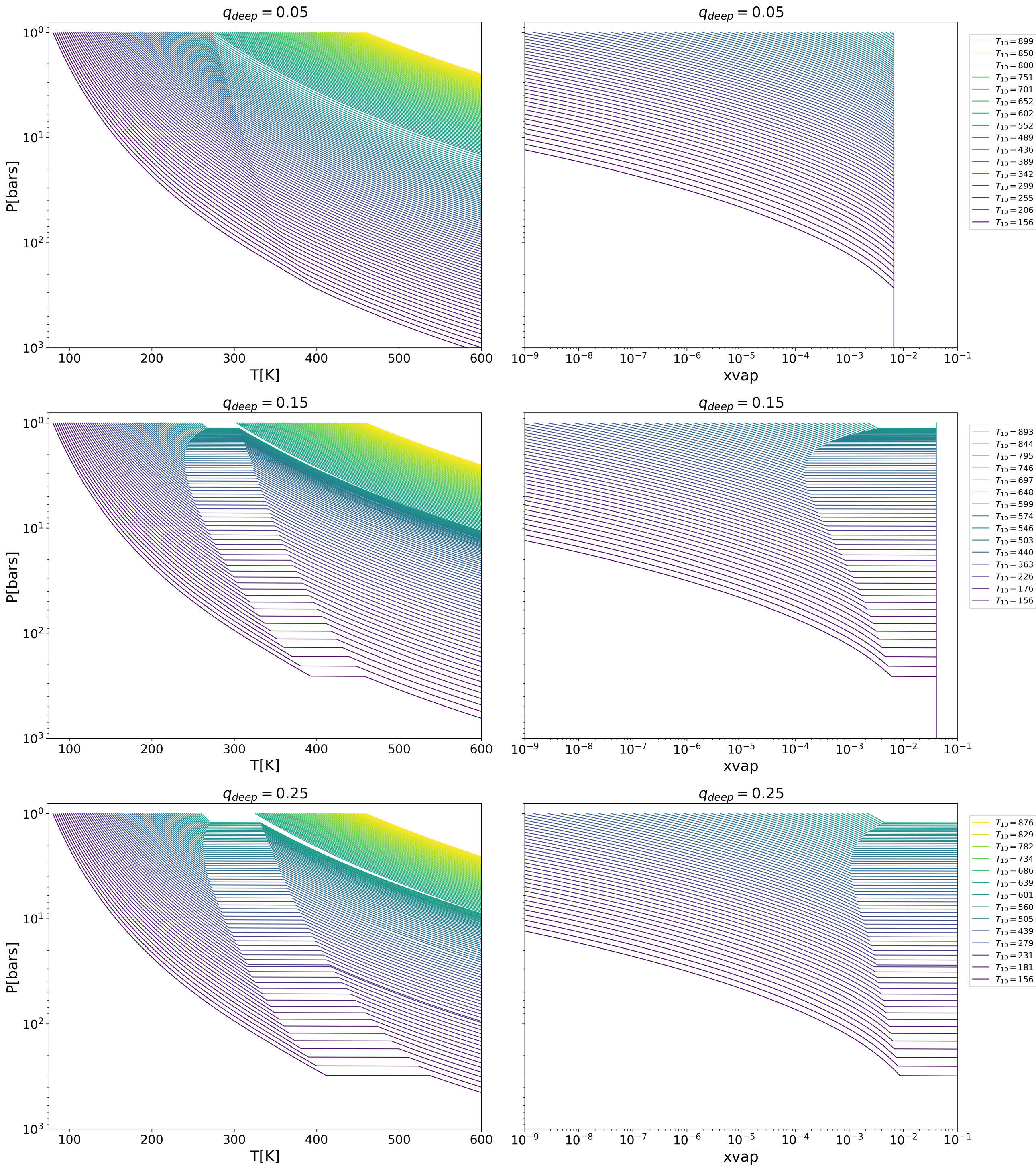

Figure 3.3: These plots were generated using our model Uranus. Again, from top to bottom, we move from $q_{\text{deep}} = 0.05$, 0.15, and 0.25, respectively. T_{10}'s range from hotter (yellow) to cooler (purple), more recent temperatures. For $q_{\text{deep}} = 0.05$, no stable radiative zones form. The kink visible in the middle of the top left plot represents the transition from a moist to dry adiabat. Condensation occurs, but no stability is achieved. For $q_{\text{deep}} = 0.15$ and $q_{\text{deep}} = 0.25$, stable radiative zones form, as indicated by the discontinuous temperature jumps moving left to right.

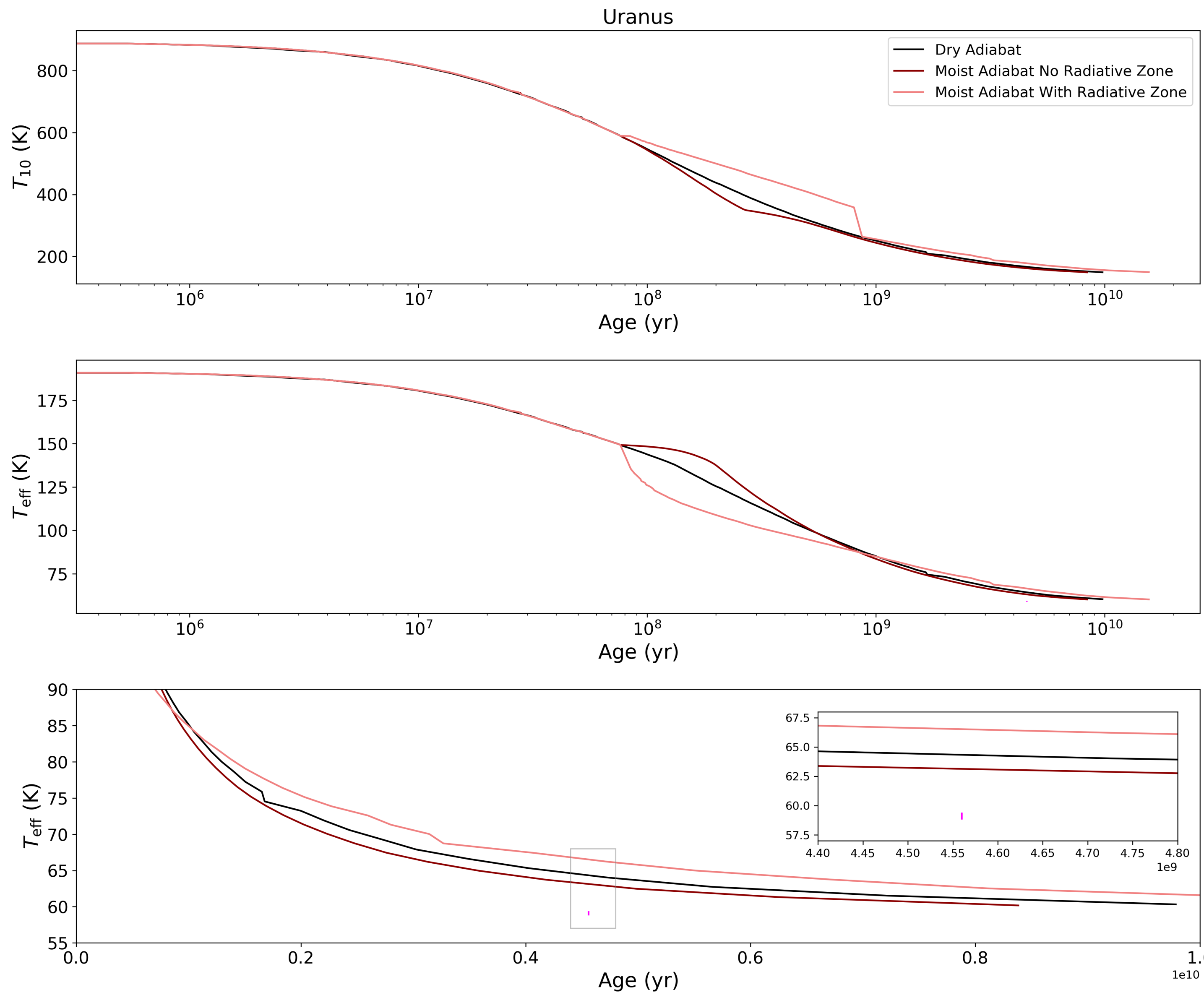

Figure 3.4: The black line represents the thermal evolution for a dry adiabat. The dark red line represents the thermal evolution for a moist adiabat that does not allow for the formation of a stable radiative layer. The light red line represents the thermal evolution of a moist adiabat that does allow for the formation of a stable radiative zone. The fuchsia dot on the lower plot represent the currently observed effective temperature of Uranus with error range.

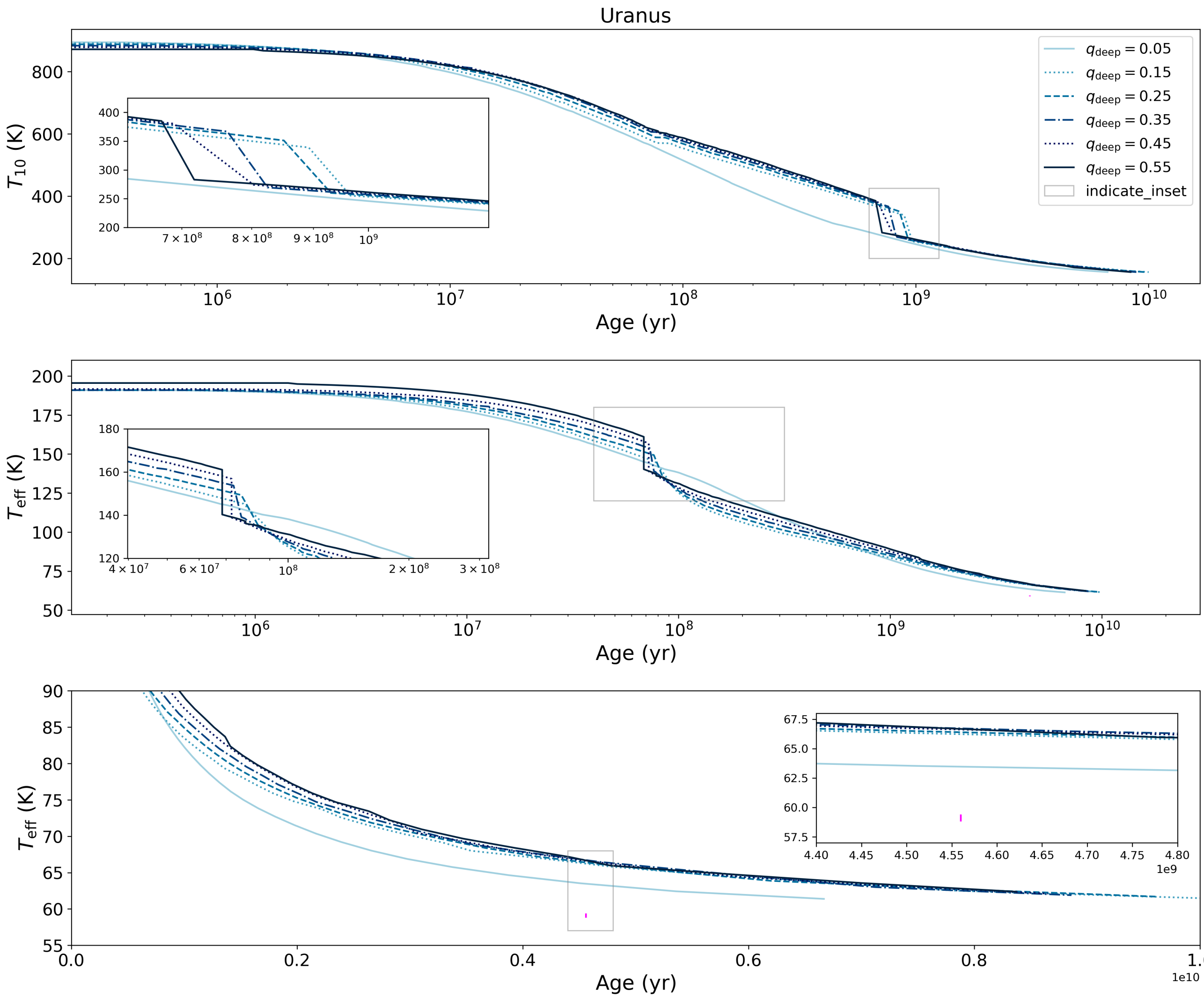

Figure 3.5: The curves in these plots represent thermal evolution tracks for different values of q_{deep}. Dark blue is the largest concentration of water vapor, at q_{deep} = 0.55 and the light blue line is the least concentration of water vapor at q_{deep} = 0.05. For q_{deep} = 0.05, there is no onset of condensation-inhibited convection and no rapid cooling episode. For larger values of q_{deep} there is a rapid cooling episode for T_{eff} at around $7x10^7$ Gyr. Similarly, a rapid cooling episode is visible deeper down in the interior as seen in the T_{10} curves at around $8x10^8$ Gyr. The insets zoom in on periods of rapid cooling. The vertical fucshia line represents the current T_{eff} with error range.

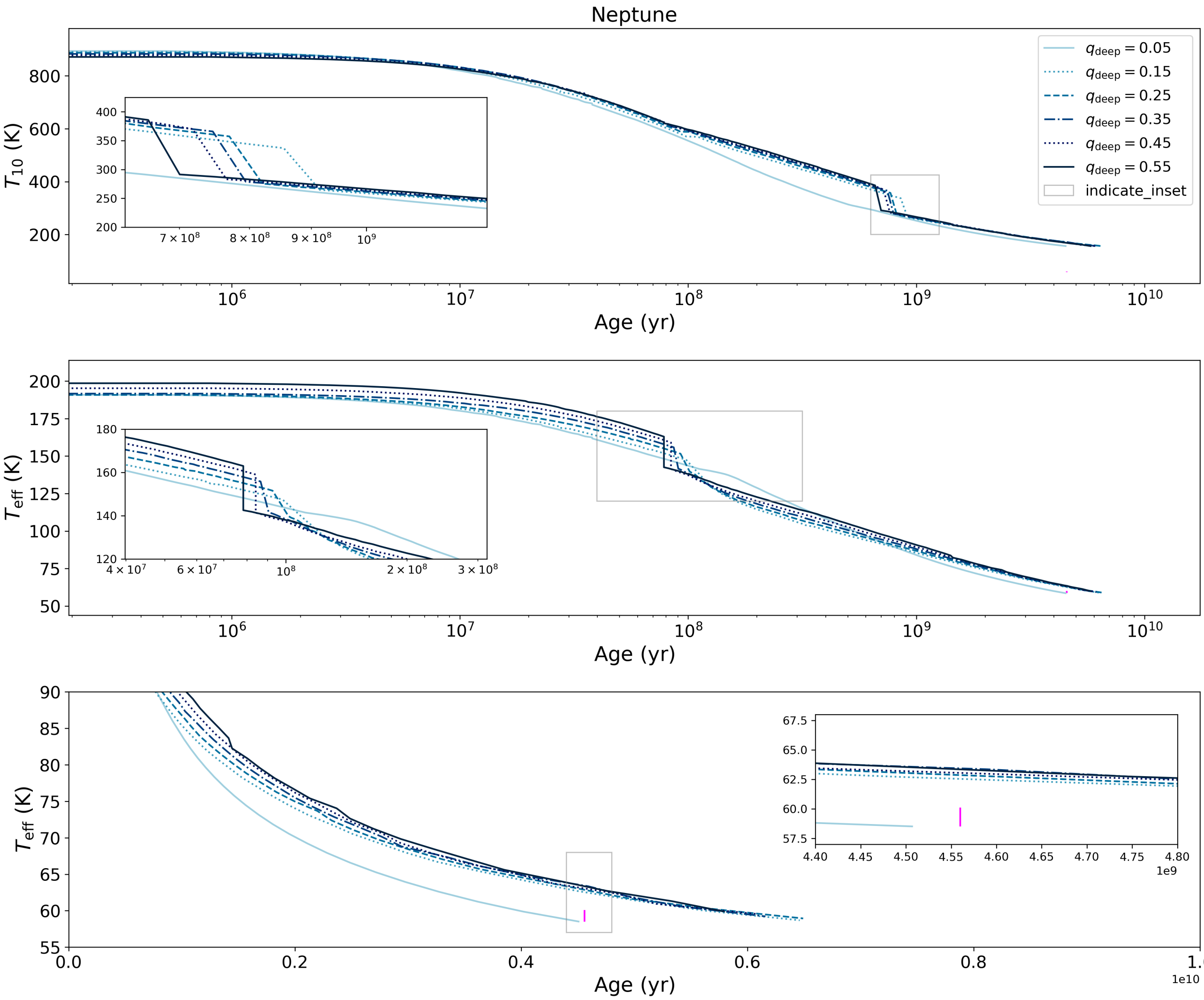

Figure 3.6: Similar to the Uranus plots, The curves in these plots represent thermal evolution tracks for different values of $q_{\rm deep}$. Dark blue is the largest concentration of water vapor, at $q_{\rm deep} = 0.55$ and the light blue line is the least concentration of water vapor at $q_{\rm deep} = 0.05$. For $q_{\rm deep} = 0.05$, there is no onset of condensation-inhibited convection and no rapid cooling episode. For larger values of $q_{\rm deep}$ there is a rapid cooling episode for $T_{\rm eff}$ at around $7x10^7$ Gyr. Similarly, a rapid cooling episode is visible deeper down in the interior as seen in the T_{10} curves at around $8x10^8$ Gyr. The insets zoom in on periods of rapid cooling. The vertical fucshia line represents the current $T_{\rm eff}$ with error range.

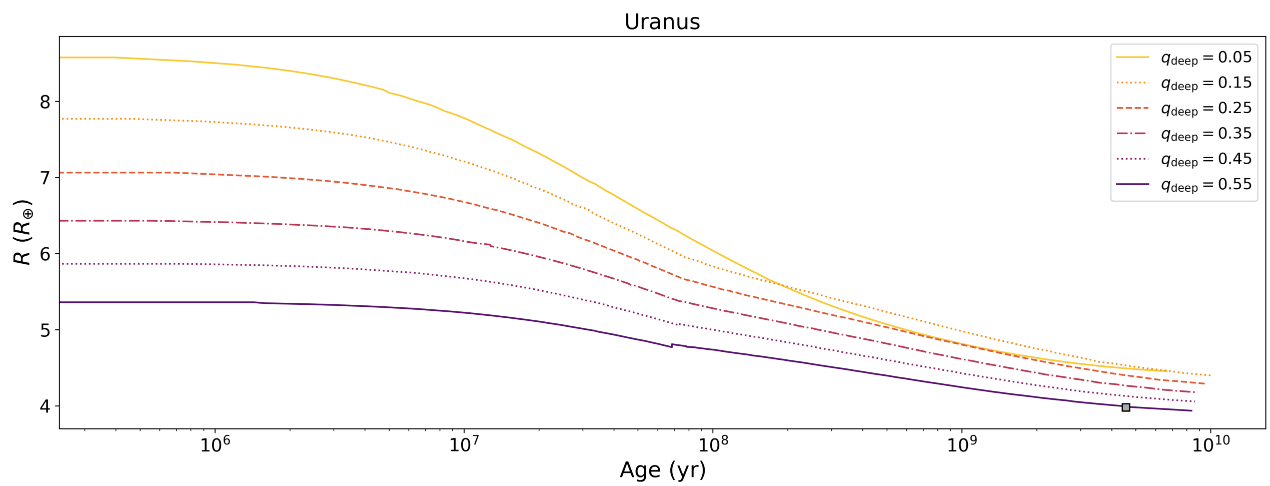

Figure 3.7: This thermal evolution plot shows the impact of different deep water concentration on the radius on model Uranus as it cools. The gray square represents the current observed radius.

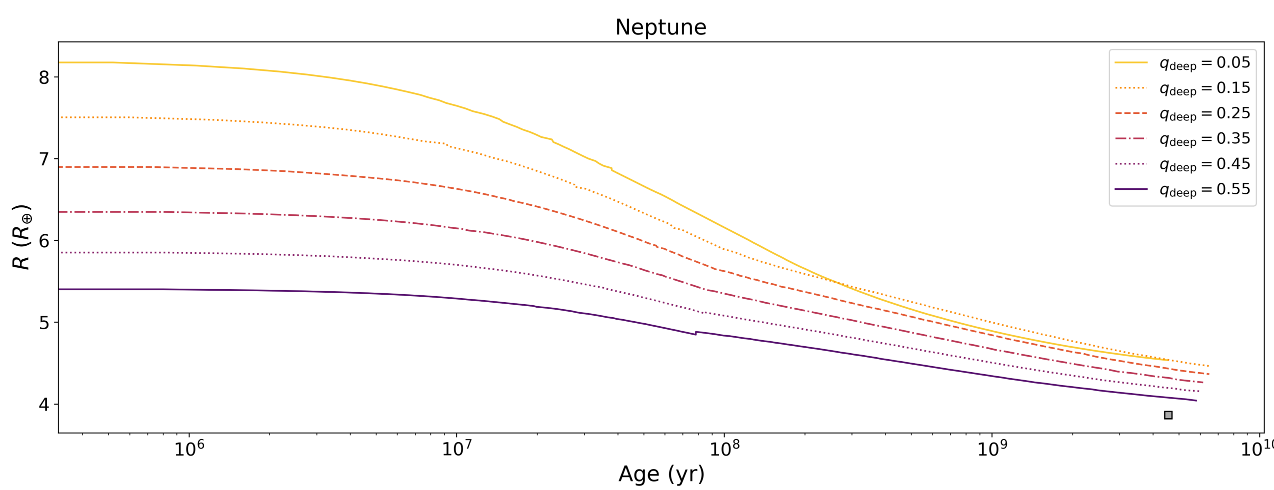

Figure 3.8: This thermal evolution plot shows the impact of different deep water concentration on the radius on model Neptune as it cools. The gray square represents the current observed radius.

4

Discussion

We set out to investigate the impact of water condensation zones on the thermal evolution of our solar system ice giants. It has been speculated that such thermal boundary layers could act as an imperfect insulator, trapping heat below and allowing the envelope above the boundary layer to cool more rapidly (Nettelmann et al., 2016)(Friedson & Gonzales, 2017)(Leconte et al., 2017)(M. Podolak, 1991)(L. Scheibe, 2019). It seems plausible that such interiors could explain the problem with Uranus appearing to have no intrinsic temperature. And, while our analysis suggests that moist-adiabatic interiors have a significant impact on the heat flow and thermal evolution of ice giants, making a case for the inclusion of moist adiabats in contemporary interior structure models, our findings are nonetheless inconclusive on the problem of Uranus. We do find that incorporating a moist adiabat into our interior structure model does result in a cooler model Uranus and Neptune than would otherwise be seen with a purely dry model. However, when we add stable radiative zones to the interior, we find in the planet's past a period of rapid cooling that results in a cooler effective temperature at around $7x10^7$ Gyr. However, both model

Uranus and model Neptune eventually become warmer at present time than predicted by either dry or simple moist adiabatic models. It is possible that reality resembles something in between the binary choice of an atmosphere with a moist adiabat containing a thermal boundary layer or an atmosphere with a moist adiabat containing no thermal boundary layer (Guillot, 2020). Our assumption of a stable shell of water condensation assumes that there are no other dynamics at play, such as upwelling or entrainment pressure (Friedson & Gonzales, 2017) eroding and punching holes in the stable radiative zone. Such a scenario could plausibly allow for more mixing of the warm gases below and above the condensation zone. Additionally, we considered only one condensate, H_2O. It would be worth considering NH_3 and CH_4, and analyzing the impact of multiple stratified layers on the cooling of the planet over time. To summarize, future work should consider: 1.) Impact of entrainment pressure on stable water condensation zones. 2.) The possibility of porous condensation zones. 3.) The formation of multiple concurrent thermal boundary layers formed from different condensates.

Bibliography

Armitage, P. J. (2013). *Astrophysics of Planet Formation*.

Chabrier, G., Mazevet, S., & Soubiran, F. (2019). A New Equation of State for Dense Hydrogen-Helium Mixtures. *Astrophysical Journal*, 872(1), 51.

Demarcus, W. C. (1958). The constitution of Jupiter and Saturn. *Astronomical Journal*, 63, 2.

Fortney, J. J. & Hubbard, W. B. (2003). Phase separation in giant planets: inhomogeneous evolution of Saturn. *Icarus*, 164(1), 228–243.

Fortney, J. J., Ikoma, M., Nettelmann, N., Guillot, T., & Marley, M. S. (2011). Self-consistent Model Atmospheres and the Cooling of the Solar System's Giant Planets. *Astrophysical Journal*, 729(1), 32.

Friedson, A. J. & Gonzales, E. J. (2017). Inhibition of ordinary and diffusive convection in the water condensation zone of the ice giants and implications for their thermal evolution. *Icarus*, 297, 160–178.

Graboske, H. C., J., Pollack, J. B., Grossman, A. S., & Olness, R. J. (1975). The structure and evolution of Jupiter: the fluid contraction stage. *Astrophysical Journal*, 199, 265–281.

Guillot, T. (1995). Condensation of Methane, Ammonia, and Water and the Inhibition of Convection in Giant Planets. *Science*, 269(5231), 1697–1699.

Guillot, T. (2020). Uranus and Neptune are key to understand planets with hydrogen atmospheres. In *European Planetary Science Congress* (pp. EPSC2020–514).

Hubbard, W. B. (1968). Thermal structure of Jupiter. *Astrophysical Journal*, 152, 745–754.

Hubbard, W. B. (1977). The Jovian Surface Condition and Cooling Rate. *Icarus*, 30(2), 305–310.

Hubbard, W. B. (1978). Comparative thermal evolution of Uranus and Neptune. *Icarus*, 35(2), 177–181.

L. Scheibe, N Nettelmann, R. R. (2019). Thermal evolution of uranus and neptune: Adiabatic models. *Astronomy and Astrophysics*, A70, 632.

Lavega, A. S. (2011). Introduction to planetary atmospheres.

Leconte, J. & Chabrier, G. (2013). Layered convection as the origin of Saturn's luminosity anomaly. *Nature Geoscience*, 6(5), 347–350.

Leconte, J., Selsis, F., Hersant, F., & Guillot, T. (2017). Condensation-inhibited convection in hydrogen-rich atmospheres . Stability against double-diffusive processes and thermal profiles for Jupiter, Saturn, Uranus, and Neptune. *Astronomy and Astrophysics*, 598, A98.

Lissauer, J. J. & Stevenson, D. J. (2007). Formation of Giant Planets. In B. Reipurth, D. Jewitt, & K. Keil (Eds.), *Protostars and Planets V* (pp. 591).

Low, F. J. (1966). Observations of Venus, Jupiter, and Saturn at $\lambda 20\ \mu$. *Astronomical Journal*, 71, 391.

M. Podolak, W.B. Hubbard, D. S. (1991). Models of uranus' interior and magnetic field. *Uranus, Editors: J.T. Bergstralh, E.D. Miner, M. Shapely Matthews*, (pp.$\tilde{2}$9).

Mankovich, C. & Fortney, J. J. (2019). Evidence for a Dichotomy in the Interior Structures of Jupiter and Saturn from Helium Phase Separation. In *AGU Fall Meeting Abstracts*, volume 2019 (pp. P24B–02).

Nettelmann, N., Wang, K., Fortney, J. J., Hamel, S., Yellamilli, S., Bethkenhagen, M., & Redmer, R. (2016). Uranus evolution models with simple thermal boundary layers. *Icarus*, 275, 107–116.

Pearl, J. C. & Conrath, B. J. (1991). The albedo, effective temperature, and energy balance of Neptune, as determined from Voyager data. *Journal of Geophysical Research*, 96, 18921–18930.

R. Kippenhahn, A. Weigert, A. W. (2012). *Stellar Structure and Evolution*. Springer.

S. Mazevet, A. Licari, G. C. & Potekhin, A. Y. (2019). Ab initio based equation of state of dense water for planetary and exoplanetary modeling. *Astronomy & Astrophysics*, A128, 621.

Sanchez-Lavega, A. (2010). *An Introduction to Planetary Atmospheres*. CRC Press.

Seager, S. (2010). Exoplanet atmospheres.

Seager, S. (2010). *Exoplanet Atmospheres: Physical Processes*.

Smoluchowski, R. (1967). Internal Structure and Energy Emission of Jupiter. *Nature*, 215(5102), 691–695.

W.B. Hubbard, D. S. (1995). The interior of neptune. *Neptune and Triton, Editor: D.P. Kruikshank*, (pp. 109).